ADVANCES IN ATMOSPHERIC SCIENCES, VOL. 33, SEPTEMBER 2016, 1047–1060

Incorporation of a Dynamic Root Distribution into CLM4.5: Evaluation of Carbon and Water Fluxes over the Amazon

Yuanyuan WANG[1,2], Zhenghui XIE[*1], and Binghao JIA[*1]

[1]*State Key Laboratory of Numerical Modeling for Atmospheric Sciences and Geophysical Fluid Dynamics, Institute of Atmospheric Physics, Chinese Academy of Sciences, Beijing* 100029

[2]*University of Chinese Academy of Sciences, Beijing* 100049

(Received 21 October 2015; revised 5 April 2016; accepted 4 May 2016)

ABSTRACT

Roots are responsible for the uptake of water and nutrients by plants and have the plasticity to dynamically respond to different environmental conditions. However, most land surface models currently prescribe rooting profiles as a function only of vegetation type, with no consideration of the surroundings. In this study, a dynamic rooting scheme, which describes root growth as a compromise between water and nitrogen availability, was incorporated into CLM4.5 with carbon–nitrogen (CN) interactions (CLM4.5-CN) to investigate the effects of a dynamic root distribution on eco-hydrological modeling. Two paired numerical simulations were conducted for the Tapajos National Forest km83 (BRSa3) site and the Amazon, one using CLM4.5-CN without the dynamic rooting scheme and the other including the proposed scheme. Simulations for the BRSa3 site showed that inclusion of the dynamic rooting scheme increased the amplitudes and peak values of diurnal gross primary production (GPP) and latent heat flux (LE) for the dry season, and improved the carbon (C) and water cycle modeling by reducing the RMSE of GPP by 0.4 g C m^{-2} d^{-1}, net ecosystem exchange by 1.96 g C m^{-2} d^{-1}, LE by 5.0 W m^{-2}, and soil moisture by 0.03 m^3 m^{-3}, at the seasonal scale, compared with eddy flux measurements, while having little impact during the wet season. For the Amazon, regional analysis also revealed that vegetation responses (including GPP and LE) to seasonal drought and the severe drought of 2005 were better captured with the dynamic rooting scheme incorporated.

Key words: CLM4.5, dynamic root distribution, carbon cycle, water cycle, Amazon

Citation: Wang, Y. Y., Z. H. Xie, and B. H. Jia, 2016: Incorporation of a dynamic root distribution into CLM4.5: Evaluation of carbon and water fluxes over the Amazon. *Adv. Atmos. Sci.*, **33**(9), 1047–1060, doi: 10.1007/s00376-016-5226-8.

1. Introduction

Roots are the primary pathway for the uptake of water and nutrients by plants and play an important role in terrestrial carbon (C) and water cycling (Nepstad et al., 1994; Jackson et al., 1997; Dickinson et al., 1998; Barlage and Zeng, 2004; Zheng and Wang, 2007). They connect the soil environment to the atmosphere through water and energy flux exchanges between the vegetation canopy and the atmosphere (Feddes et al., 2001). Root vertical distribution, one of the most important properties of roots, is an essential component of many eco-hydrological models (Lai and Katul, 2000) and land surface models (LSMs) (Zeng et al., 1998; Feddes et al., 2001; El Maayar and Sonnentag, 2009); it mainly controls the extent of root water uptake among soil layers, and therefore soil water stress. The soil water stress further influences transpiration, C assimilation, and subsequently other C and water fluxes (Bonan, 1996; Zeng et al., 2002; Ivanov et al., 2008). Thus, a realistic representation of root distribution is very important for hydrological, ecological and climate modeling (Zheng and Wang, 2007; Jing et al., 2014).

As a consequence of a lack of appropriate global root datasets owing to the difficulty of measuring entire root distributions throughout the soil profile (Jing et al., 2014; Warren et al., 2015), the description of root distributions in LSMs is often simplified or ignored (Zeng et al., 2002; Warren et al., 2015). In most LSMs, root distribution is treated as a static component, and three rooting parameterizations are widely used. The first is a one-parameter asymptotic root equation, proposed by Jackson et al. (1996), which describes root distribution decreasing exponentially with depth. It has been used in NCAR's LSM (Bonan, 1996) and the Simple Biosphere Model (Baker et al., 2008). The second is a two-parameter asymptotic root distribution decreasing exponentially with depth (Zeng, 2001), which is used in NCAR's CLM (Oleson et al., 2010, 2013). And the third is a logistic dose-response curve root profile proposed by Schenk and Jackson (2002), which has two shape parameters that describe the soil depth above which 50% and 95% of the root mass occurs. This parameterization is employed in the Conjunctive Surface–Subsurface Process Model (Yuan and

* Corresponding author: Binghao JIA
Email: bhjia@mail.iap.ac.cn

Liang, 2011) and Mechanistic Multilayer Canopy–Soil–Root System Model (Drewry et al., 2010; Le et al., 2012). All parameters in these three root distribution schemes depend only on vegetation types, with root distributions spatially and temporally invariant. However, substantial differences in root distributions are apparent even for the same type of vegetation, as determined from measuring root profiles in different irrigation and fertilization experiments (Weaver, 1926; Li et al., 1998; Fan et al., 2012). Furthermore, it has been demonstrated that plants tend to allocate C to enhance the acquisition of a limited resource (Hutchings and de Kroon, 1994), and thus tend to grow more roots in zones where soil moisture is more freely available, especially when suffering from water deficit (Coelho and Or, 1999; Collins and Bras, 2007; Sivandran and Bras, 2013), and where more nutrients can be acquired (McMurtrie et al., 2012). These aspects imply that root systems have the plasticity to dynamically respond to environmental conditions, such as water and nutrient availability (Schenk and Jackson, 2002; Hodge, 2004; Schenk, 2008; Smithwick et al., 2014; El Masri et al., 2015), indicating that the three rooting schemes mentioned above are insufficient in their representation of the actual root distribution, and thus need to be improved.

In this study, a dynamic root distribution scheme that describes root growth as a compromise between water and nitrogen (N) availability, was implemented in CLM4.5 (Oleson et al., 2013). The respective impacts on terrestrial C and water cycles were evaluated over the Amazon. The evaluation focused on the model prognostic skill with respect to gross primary production (GPP), net ecosystem exchange (NEE), latent heat flux (LE) and soil water content (SWC). Section 2 describes the model development, study area, experimental design and data used. Results are given in section 3, followed by conclusions and discussion in section 4.

2. Methods

2.1. *Model development*

2.1.1. *CLM4.5*

CLM4.5, a state-of-the-art LSM, is the latest version of the CLM family of models and the land component of CESM1.2 (Oleson et al., 2013). It succeeds CLM4, with updates to the photosynthesis, soil biogeochemistry, fire dynamics, cold region hydrology, lake model, and biogenic volatile organic compounds model (Li et al., 2013). The spatial heterogeneity of the land surface is represented in CLM as a nested sub-grid hierarchy, and vegetation is classified into 16 plant functional types (PFTs) according to different photosynthesis parameters and optical properties (leaf and stem reflectance and transmittance in visible and near-infrared wavebands). The soil columns have 15 vertical layers, but hydrology calculations are only made for the top 10 layers. CLM4.5 also has an option to run with an interactive C–N (CN) cycle (denoted as CLM4.5-CN), which is fully prognostic with respect to all C and N state variables in vegetation, litter and soil organic matter. When the CN biogeochemistry module is active, N limitation on photosynthesis is prognostic and leaf area, stem area indices and vegetation heights are all determined prognostically by the model (Lawrence et al., 2011). A detailed description of its biogeophysical and biogeochemical parameterizations and numerical implementation is given in Oleson et al. (2013).

A root distribution function determines the fraction of roots in each soil layer. CLM4.5 uses the root distribution equation of Zeng (2001):

$$r_i = \begin{cases} 0.5\left[\begin{array}{l}\exp(-r_a z_{h,i-1}) + \exp(-r_b z_{h,i-1}) - \\ \exp(-r_a z_{h,i}) - \exp(-r_b z_{h,i})\end{array}\right] & \text{for } 1 \leqslant i < 10 \\ 0.5[\exp(-r_a z_{h,i-1}) + \exp(-r_b z_{h,i-1})] & \text{for } i = 10 \end{cases}, \quad (1)$$

where $z_{h,i}$ (m) is the depth from the soil surface to the interface between layer i and $i+1$, and r_a and r_b are two PFT-dependent root parameters.

2.1.2. *Dynamic rooting scheme and its implementation*

At present, although the root C pool does vary temporally, due to the static rooting scheme there is no net change to the root fraction within each soil layer. To represent actual root growth in CLM4.5 dynamically, we adopted a dynamic rooting scheme proposed by Hatzis (2010), which allows the total new root C gain at each time step to dynamically allocate to each soil layer according to the surrounding environment, i.e. a compromise between soil water and soil mineral N, as expressed by Eq. (2):

$$\Delta C_{\mathrm{fr},i} = \Delta C_{\mathrm{fr}} \left[(1-\beta_{\mathrm{t}}) \frac{w_i \Delta z_i}{\sum_{i=1}^{10} w_i \Delta z_i} + \beta_{\mathrm{t}} \frac{n_i \Delta z_i}{\sum_{i=1}^{10} n_i \Delta z_i} \right], \quad (2)$$

where ΔC_{fr} (units: g C m^{-2} s^{-1}) is the newly assimilated C allocated to roots, Δz_i (units: m) is the soil layer thickness, n_i (units: g N m^{-3}) is soil mineral N content, and w_i is the plant wilting factor of layer i. β_{t} is the soil water stress due to water deficiency, depending on w_i and root fraction (r_i), expressed as:

$$\beta_{\mathrm{t}} = \sum_{i=1}^{10} w_i r_i \,, \quad (3)$$

$$w_i = \max\left(0, \min\left[1, \frac{\psi_{\mathrm{c}} - \psi_i}{\psi_{\mathrm{c}} - \psi_{\mathrm{o}}} \frac{\theta_{\mathrm{sat},i} - \theta_{\mathrm{ice},i}}{\theta_{\mathrm{sat},i}}\right]\right), \quad (4)$$

where ψ_i is the soil water matric potential (units: mm), and ψ_{c} and ψ_{o} are the soil water potential (units: mm) when stomata are fully closed or fully open, respectively. $\theta_{\mathrm{sat},i}$ and $\theta_{\mathrm{ice},i}$ are the saturated volumetric water and ice content, respectively (units: m^3 m^{-3}). The function β_{t} ranges from 0 to 1, with larger values indicating higher water availability. The root distribution after the new dynamic allocation is then updated, based on the root C ($C_{\mathrm{fr},i}$; units: g C m^{-2}) of layer i and the total root C ($\sum_{i=1}^{10} C_{\mathrm{fr},i}$; units: g C m^{-2}):

$$r_i = \frac{C_{\mathrm{fr},i}}{\sum_{i=1}^{10} C_{\mathrm{fr},i}} \,. \quad (5)$$

To incorporate this scheme into CLM4.5, the total N (TN) data from the Global Soil Dataset for Earth System Mod-

eling, developed by the Land–Atmosphere Interaction Research Group at Beijing Normal University, were used to replace the vertical soil mineral N content, as the vertically resolved soil mineral N is not predicted in CLM4.5. The TN data have a resolution of 30 arc-seconds, with the vertical variation captured by eight layers to a depth of 2.3 m (i.e. 0–0.045, 0.045–0.091, 0.091–0.166, 0.166–0.289, 0.289–0.493, 0.493–0.829, 0.829–1.383 and 1.383–2.296 m), consistent with the vertical layers of CLM4.5 (Shangguan et al., 2014). Here, we up-scaled the TN data from 30 arc-seconds to 0.5° by means of an area-weighted average and used linear regressions (Hatzis, 2010) to estimate TN values for the residual two layers.

The dynamic rooting scheme influences the eco-hydrological modeling in CLM4.5 in multiple ways (Fig. 1). First, the varying root distribution has a direct impact on β_t, as in Eq. (3). On the one hand, β_t influences photosynthesis by multiplying it by the maximum catalytic capacity of the Rubisco enzyme (V_{cmax}). On the other hand, β_t further influences plant transpiration through stomatal conductance, as stomatal conductance is linearly related to β_t in the model. Second, the varying root fraction influences the calculation of the effective root fraction, which affects the water extracted from each layer, and therefore the SWC. In addition, the soil N plays an important part, it not only influences root fraction, as Eq. (2) shows, but also controls the amount of N that can be absorbed by plants, and thus limits photosynthesis.

2.2. *Study area*

The Amazon region shown with a black border in Fig. 2 (Zeng et al., 2008; Marthews et al., 2014), which contains about 50% of the world's tropical forests, is crucial to global hydrological and C cycles, and changes in its biophysical state can exert a strong influence on global climate (Baker et al., 2008). It is mainly covered by tropical broadleaf evergreen tree (BET Tr), tropical broadleaf deciduous tree (BDT Tr), C_3 grass (C_3 NA) and C_4 grass (C_4) (Fig. 2a), according to MODIS land cover data in CLM4.5 (Lawrence and Chase, 2007). The driving climatic forcing of energy, water and C cycles in the Amazon is the spatial and temporal distribution of precipitation (Ichii et al., 2007). The dry seasons are usually defined as months with less than 100 mm precipitation (Baker et al., 2008). Mean monthly precipitation in the Amazon (Fig. 2b) is 185.35 mm month^{-1}, with a range of 29.14–372.64 mm month^{-1}, based on CRU–NCEP reanalysis data (CRUNCEP) from 1982–2010 (Viovy, 2011). The dry season length increases from the northwestern to southeastern Amazon, along with a transition from evergreen broadleaf forest to deciduous broadleaf forest and C_4 grass (Fig. 2c).

The Large Scale Biosphere–Atmosphere Experiment (LBA) in the Amazon (Avissar et al., 2002) monitored water, energy and C exchange between ecosystems and the atmosphere. BRSa3 (3.02°S, 54.97°W) is a typical site of LBA, located within the Tapajos National Forest, Pará, Brazil (Fig. 2b), covered by BET Tr. During the study period of 2001–2003, the mean annual air temperature and solar radiation were 25.9°C and 188.7 W m^{-2}, respectively. The mean annual total precipitation was 1658 mm, with less rainfall during the dry season of July–December (Fig. 3). The seasonal variation of monthly air temperature was quite small (<2°C) and the solar radiation of the dry season was slightly higher than that of the wet season. At BRSa3, an eddy covariance system was installed to measure the fluxes of carbon dioxide, LE and all meteorological variables required for running CLM4.5.

2.3. *Experimental design and data*

Two pairs of experiments were conducted to study the effects of dynamic root distribution on eco-hydrological modeling: one for the BRSa3 site and the other for the Amazon region. For each pair of experiments, two offline simulations were conducted, both with CLM4.5-CN: simulations using the default model (control run, "CTL") and the model with dynamic root distribution (new run, "NEW"). For estab-

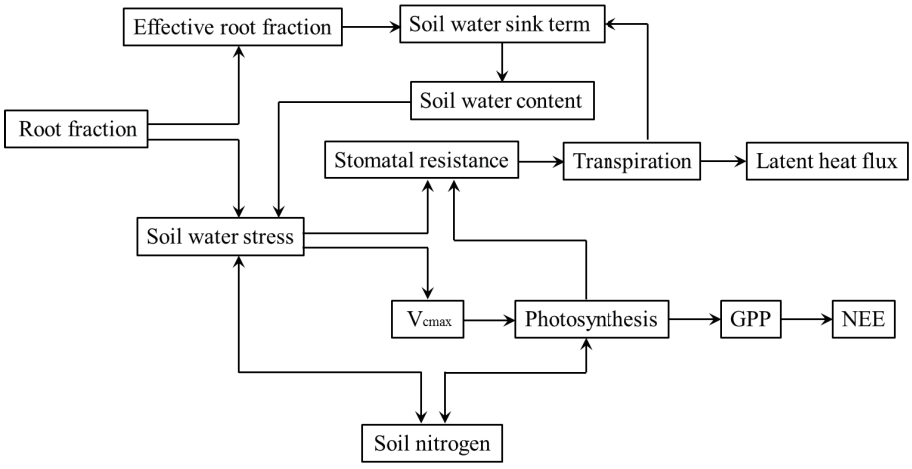

Fig. 1. Conceptual diagram of the impacts of a dynamic root distribution on eco-hydrological modeling in CLM4.5.

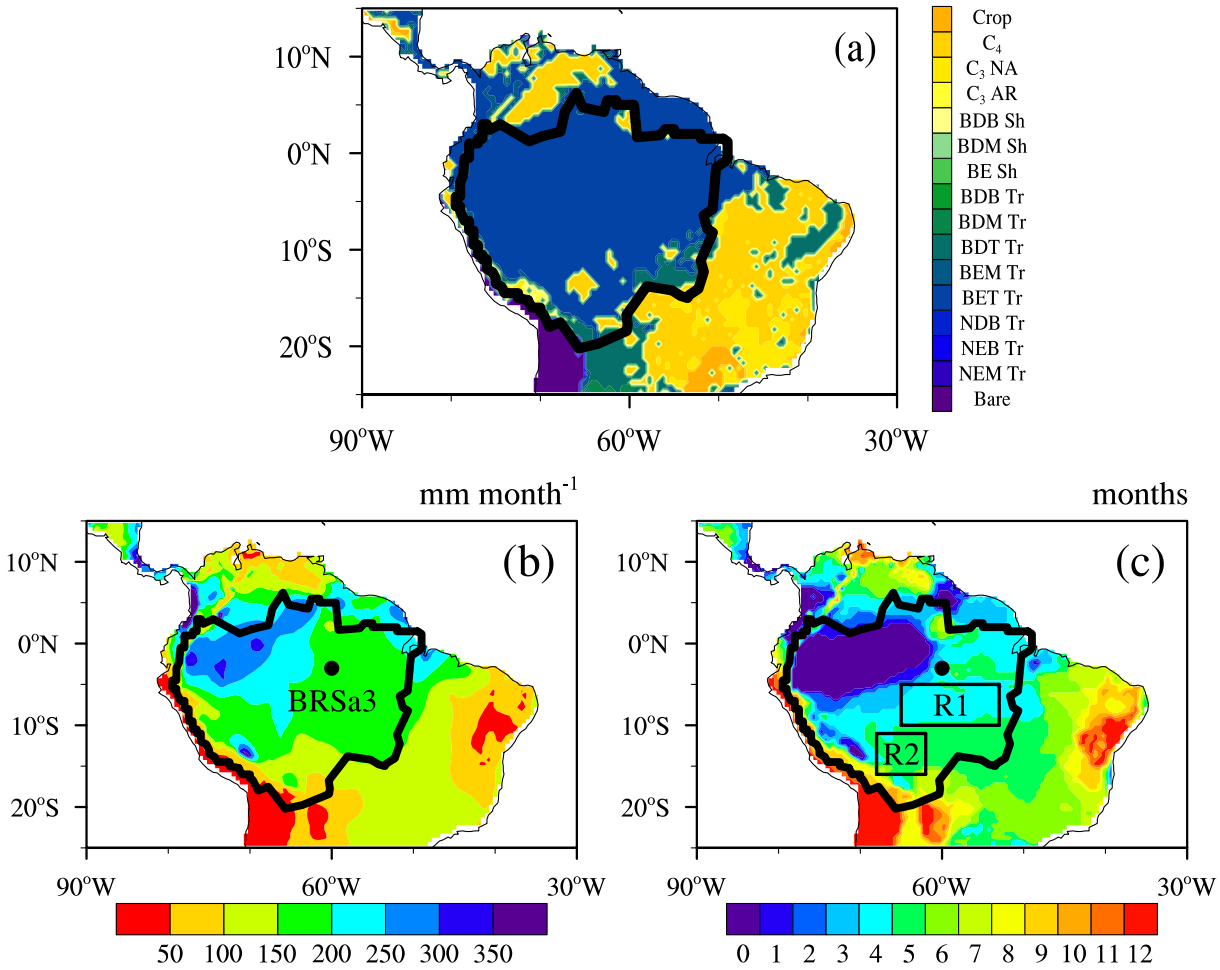

Fig. 2. (a) The dominant PFTs in the Amazon [bare soil (Bare); temperate needleleaf evergreen tree (NEM Tr); boreal needleleaf evergreen tree (NEB Tr); boreal needleleaf deciduous tree (NDB Tr); tropical broadleaf evergreen tree (BET Tr); temperate broadleaf evergreen tree (BEM Tr); tropical broadleaf deciduous tree (BDT Tr); temperate broadleaf deciduous tree (BDM Tr); boreal broadleaf deciduous tree (BDB Tr); temperate broadleaf evergreen shrub (BE Sh); temperate broadleaf deciduous shrub (BDM Sh); boreal broadleaf deciduous shrub (BDB Sh); C3 arctic grass (C3 AR); C3 grass (C3 NA); C4 grass (C4); and Crop]. (b) Average monthly (1982–2010) precipitation (units: mm month^{-1}) over the Amazon according to CRUNCEP, and the location of Tapajos National Forest km8 (BRSa3). (c) Number of dry months per year, defined as monthly precipitation less than 100 mm (the two black boxes represent the two study areas analyzed in section 3.2, denoted as R1 and R2, respectively). The border of the Amazon is shown as a black line.

lishing the C and N pools and fluxes (Castillo et al., 2012; Hudiburg et al., 2013), the 1200-year spun-up results were used as initial conditions for both site-level and regional simulations (e.g. the soil C pool of the BRSa3 site was initialized from 0 to about 5.89 kg C m^{-2}). The two simulations of each pair of experiments shared the same initial conditions, thus eliminating changes other than those from dynamic root distribution (Yan and Dickinson, 2014).

For this study, half-hourly, daily and monthly gap-filled observations at the BRSa3 site were downloaded from FLUXNET (www.fluxdata.org). For site-level simulations, the meteorological data, including wind speed, 2-m air temperature, specific humidity, air pressure, incident solar radiation and precipitation, measured at 30-min intervals at the BRSa3 site during 2001–03, were used to force the offline simulations. Observed GPP, NEE, LE and SWC (mean of SWC measured at 10 and 20 cm), corresponding with the study period, were used to assess the models' abilities.

For the regional case, CRUNCEP was used as the atmospheric forcing. This is a 110-year (1901–2010) observation-based atmospheric forcing dataset, which is a combination of two existing datasets: the CRU TS3.2 $0.5^\circ \times 0.5^\circ$ monthly data covering the period 1901–2002, and the NCEP reanalysis $2.5^\circ \times 2.5^\circ$ six-hourly data from 1948 to 2010 (Viovy, 2011). The dataset comprises six-hourly data on precipitation, solar radiation, air temperature, pressure, humidity and wind. We utilized CRUNCEP for 1901–81 in the spun-up simulation and results for 1982–2010 at a $0.5^\circ \times 0.5^\circ$ resolution. Since evaluating GPP and LE from LSMs at regional scales is hindered by a lack of extensive observations, two products were used as reference for benchmarking our comparisons in the Amazon region: the global GPP (monthly,

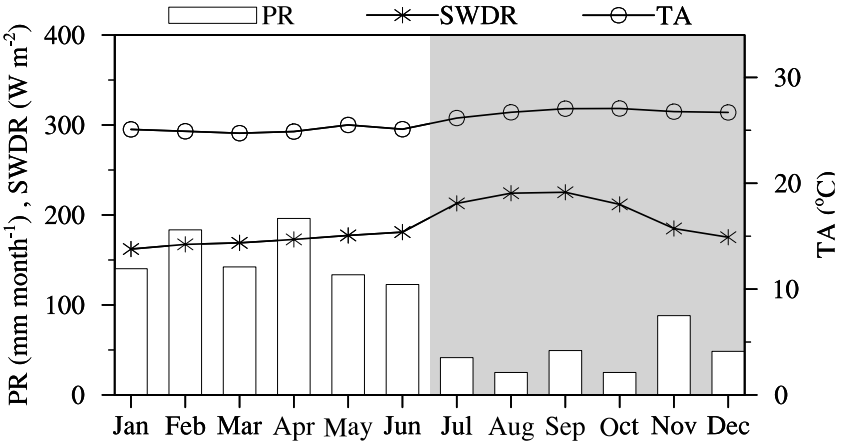

Fig. 3. Average monthly precipitation (PR; units: mm month^{-1}; bars), shortwave downward radiation (SWDR; units: W m^{-2}; solid line with asterisks) and air temperature (TA; units: °C; solid line with circles) at the BRSa3 site according to observations from 2001–03 (grey area indicates the dry season).

$0.5^\circ \times 0.5^\circ$) and LE (monthly, $0.5^\circ \times 0.5^\circ$), up-scaled from FLUXNET observations using the machine learning technique, and model tree ensembles (MTE) data for 1982–2010 (Jung et al., 2009, 2011).

2.4. *Mathematical Indices for Model's Performance*

To evaluate the agreement between model simulations and observations, four indices were used: agreement index (d) (Li et al., 2012), correlation coefficient (R), mean bias error (MBE) and root mean square error (RMSE), defined as follows:

$$R = \frac{\sum_{i=1}^{N}(x_{\mathrm{sim},i} - \overline{x}_{\mathrm{sim}})(x_{\mathrm{obs},i} - \overline{x}_{\mathrm{obs}})}{\sqrt{\sum_{i=1}^{N}(x_{\mathrm{sim},i} - \overline{x}_{\mathrm{sim}})^2}\sqrt{\sum_{i=1}^{N}(x_{\mathrm{obs},i} - \overline{x}_{\mathrm{obs}})^2}}, \quad (6)$$

$$\mathrm{MBE} = \frac{\sum_{i=1}^{N}(x_{\mathrm{sim},i} - x_{\mathrm{obs},i})}{N}, \quad (7)$$

$$\mathrm{RMSE} = \sqrt{\frac{\sum_{i=1}^{N}(x_{\mathrm{sim},i} - x_{\mathrm{obs},i})^2}{N}}, \quad (8)$$

$$d = 1 - \frac{\sum_{i=1}^{N}(x_{\mathrm{sim},i} - x_{\mathrm{obs},i})^2}{\sum_{i=1}^{N}(|x_i - \overline{x}_{\mathrm{obs}}| + |x_{\mathrm{obs},i} - \overline{x}_{\mathrm{obs}}|)^2}, \quad (9)$$

where x_{sim} is model simulation either from CTL or NEW, x_{obs} is the corresponding observation, $\overline{x}_{\mathrm{sim}}$ and $\overline{x}_{\mathrm{obs}}$ are the mean of x_{sim} and x_{obs}, respectively. For d, a value of 1 indicates a perfect match and 0 indicates no agreement at all. RMSE provides an estimate of the absolute bias in the model simulation and the smaller the value of RMSE, the better the agreement between the simulation and observation is.

3. Results

For optimal evaluation of the effects of a dynamic root distribution on eco-hydrological modeling, the diurnal cycles of β_t, GPP, NEE, LE and SWC (mean of the top 20 cm) for the wet (April) and dry (October) seasons at the BRSa3 site are presented in Fig. 4, together with their corresponding climate variables (precipitation, solar radiation and temperature). GPP and LE in from CTL and NEW showed the same diurnal cycle as observed, with a peak value at noon (Figs. 4e, g, m and o), which was mainly driven by solar radiation (Figs. 4b and j). Furthermore, the two simulations did not differ from one another regarding GPP and LE during the wet season, which had sufficient rainfall (Fig. 4a) for no soil water stress ($\beta_t = 1$; Fig. 4d), and agreed well with observation. However, during the dry season, with little precipitation (Fig. 4i) and thus severe water stress ($\beta_t < 0.8$; Fig. 4l), CTL obviously underestimated daytime GPP (~40% at noon; Fig. 4m) and LE (typically >20% around noon; Fig. 4o). By incorporating the dynamic rooting scheme in NEW, more root C was allocated into deeper soil layers (Fig. 5). Compared with the observed root distribution data (Jackson et al., 1996), the dynamic root scheme realistically captured the observed root profile, better than the static root distribution, with the largest fraction of roots in deep layers, and thus more water could be taken up by roots. This further reduced the soil water stress (Fig. 4l), and so the amplitudes and peak values of GPP (Fig. 4m) and LE (Fig. 4o) for the dry season increased. That said, part of the underestimation still remained, indicating that other mechanisms apart from the dynamic rooting scheme still need to be considered.

NEE is an expression of net C exchange between ecosystem and atmosphere, with positive values indicating efflux into the atmosphere and negative values indicating uptake by the biosphere, calculated as per Eq. (10):

$$\begin{aligned}\mathrm{NEE} &= -(\mathrm{GPP} - \mathrm{ER}) = -(\mathrm{GPP} - \mathrm{AR} - \mathrm{HR}) \\ &= -(\mathrm{GPP} - \mathrm{GR} - \mathrm{MR} - \mathrm{HR}), \end{aligned} \quad (10)$$

where GR is the growth respiration, MR is the maintenance respiration, HR is the heterotrophic respiration, AR is the autotrophic respiration (AR = GR + MR), and ER is the total ecosystem respiration (ER = AR + HR). For the wet season, both the two runs captured the amplitudes and peak value of

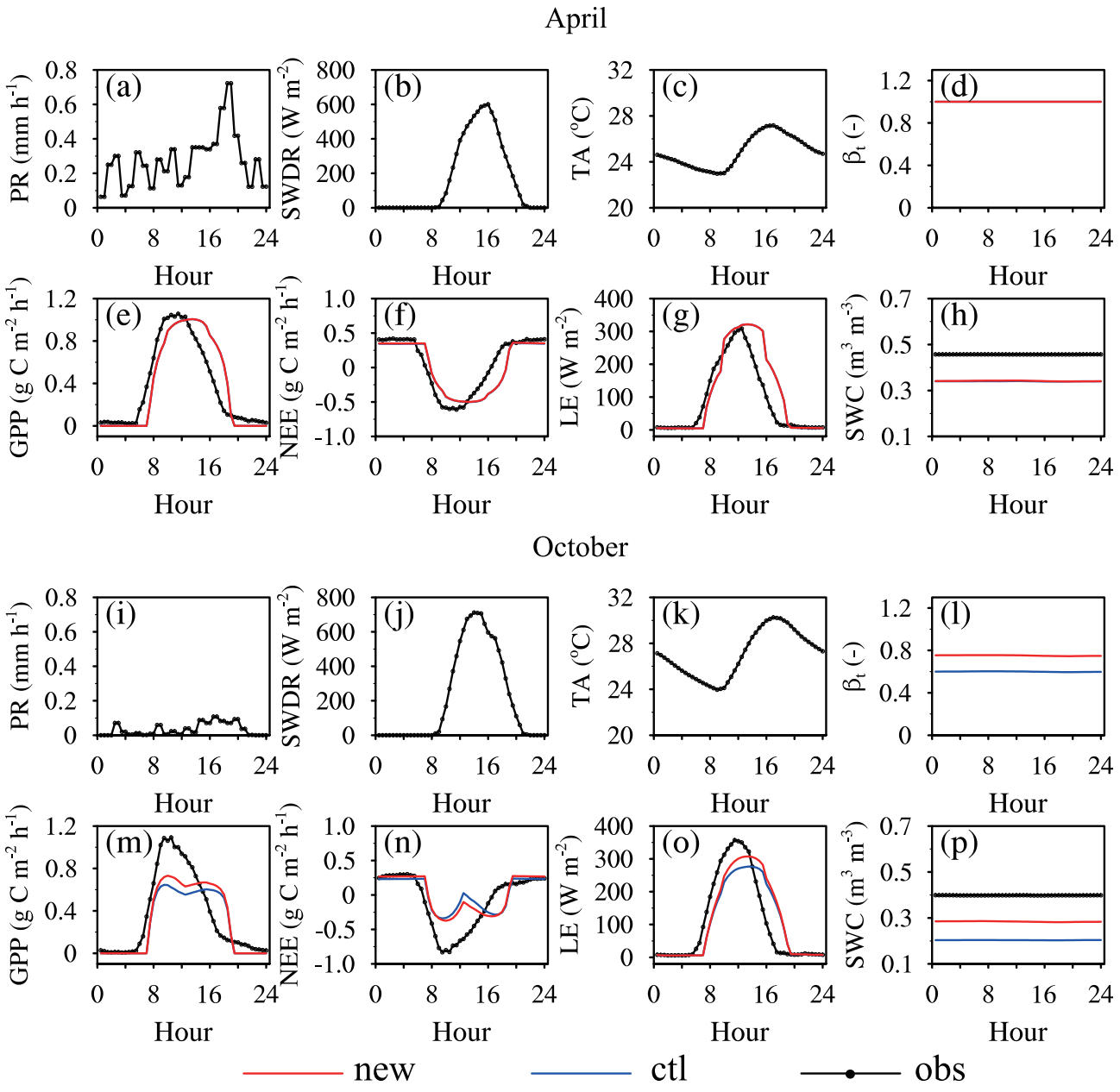

Fig. 4. Diurnal (a) precipitation (PR; units: mm h^{-1}), (b) shortwave downward radiation (SWDR; units: W m^{-2}), (c) air temperature (TA; units: °C), (d) β_t, (e) GPP (units: g C m^{-2} h^{-1}), (f) NEE (units: g C m^{-2} h^{-1}), (g) LE (units: W m^{-2}) and (h) SWC (mean of 0–20 cm units: m^3 m^{-3}) for wet (April) months at the BRSa3 site, aggregated over 2001–03. Panels (i–p) are the same as panels (a–h) but for the dry (October) season.

observed NEE well, with the biosphere acting as a C source in the morning and evening, but a C sink at noon (Fig. 4f). However, for the dry season, CTL greatly underestimated the peak value of C uptake at noon (Fig. 4n), due to the severe water stress. However, during the dry season, GR, MR and HR all increased due to the increase in photosynthesis, which then led to higher ER (not shown). Because GPP increased more than ER, the NEE values (negative) became smaller, and thus NEW improved the simulation of NEE, with more C uptake at noon, closer to that observed.

For the limited SWC observation, just the mean value of SWC from the top layers (0–20 cm) of the two runs was compared with observation (Figs. 4h and p). SWC showed little diurnal variation and was underestimated both for the dry and wet seasons — more severely for the dry season. The underestimation of SWC for the top layers in the dry season was slightly reduced in NEW (Fig. 4p), because the dynamic rooting scheme allowed the roots to absorb water from the deep soil (Fig. 5). However, despite improvement due to the incorporation of a dynamic root distribution, significant biases in SWC simulations remained.

Figures 6a–e show the mean daily β_t, GPP, NEE, LE and SWC (0–20 cm), respectively, averaged for 2001–03, and the differences in GPP, NEE, LE and SWC between the

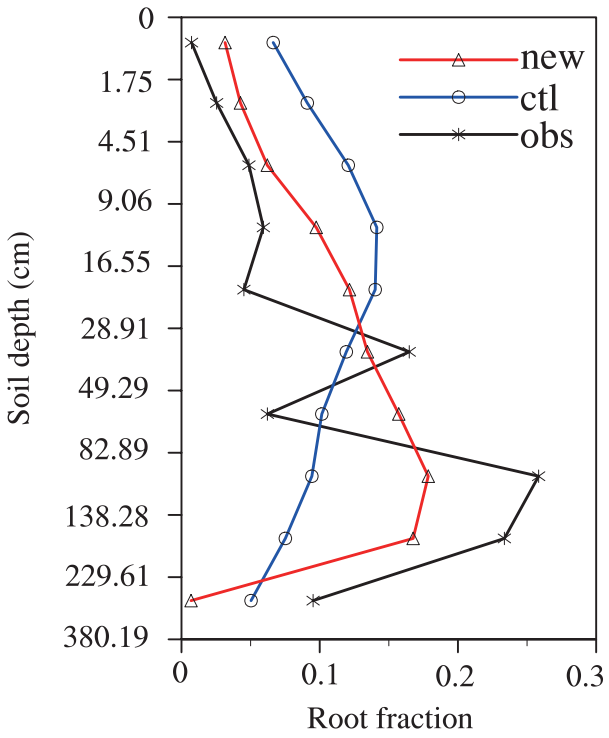

Fig. 5. Mean root profile over the 3-year (2001–03) simulations of the two runs.

two runs were all significant at the 95% confidence level according to the Student's *t*-test. Decreases in GPP and LE for July–December (Figs. 6b and d) due to dryness ($\beta_t < 1$; Fig. 6a) were found in CTL, which were much lower than observed, possibly caused by the model's excessive sensitivity to drought (Baker et al., 2008). However, NEW, with its dynamic rooting scheme, improved the simulation for GPP and LE during the dry season, which were closer to their corresponding observations, by reducing the underestimation of GPP and LE by higher β_t (lower soil water stress), resulting in lower MBE (Figs. 7b and j) and RMSE (Figs. 7c and k). For NEE, CTL simulated positive values during the dry season, indicating the biosphere acted as a C source, contrary to observation (Fig. 6c). When a dynamic root distribution was considered, the biosphere was altered to a C sink or the magnitude of C emissions was reduced for July–December, which was closer to observations. This reduced the MBE from 1.25 to 0.40 g C m^{-2} d^{-1} (Fig. 7f) and the RMSE from 3.91 to 1.95 g C m^{-2} d^{-1} (Fig. 7g). For the mean SWC of the top 0–20 cm, both runs gave large underestimations. However, NEW reduced the underestimation for July–December, with the RMSE lowered from 0.18 to 0.15 m^3 m^{-3}, as the dynamic root distribution allowed roots to absorb more water from deeper soil layers (Fig. 6e). Overall, GPP, NEE, LE and SWC were better estimated using the new model, with lower MBE and RMSE and higher *R* and *d*, especially during dry months.

To further evaluate how a dynamic root distribution affects the response of terrestrial C and water cycles to seasonal droughts in the Amazon, two study regions (denoted R1 and R2), dominated by BET Tr and C_4 grass, respectively, were selected for analysis (Fig. 2c). The mean monthly precipitation for R1 and R2 was 180.48 and 136.35 mm $month^{-1}$,

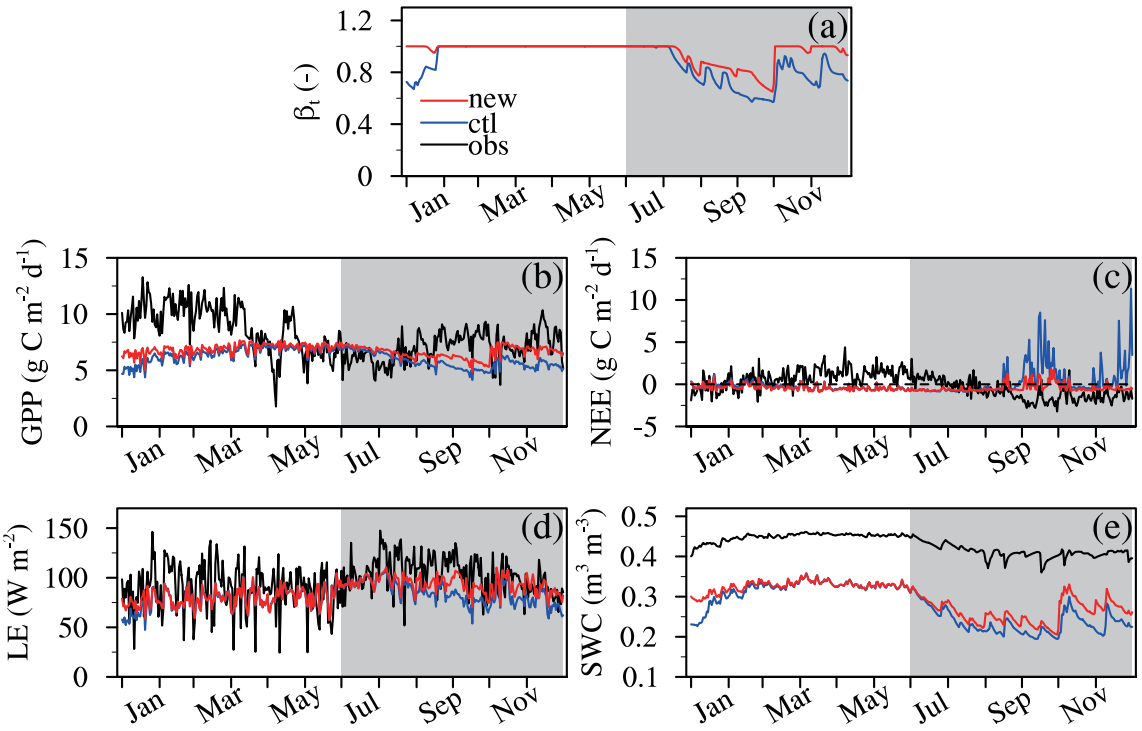

Fig. 6. Difference among the simulated mean daily values of (a) β_t, (b) GPP, (c) NEE, (d) LE and (e) SWC (mean of 0–20 cm) at the BRSa3 site averaged from 2001 to 2003 (grey areas indicate the dry season).

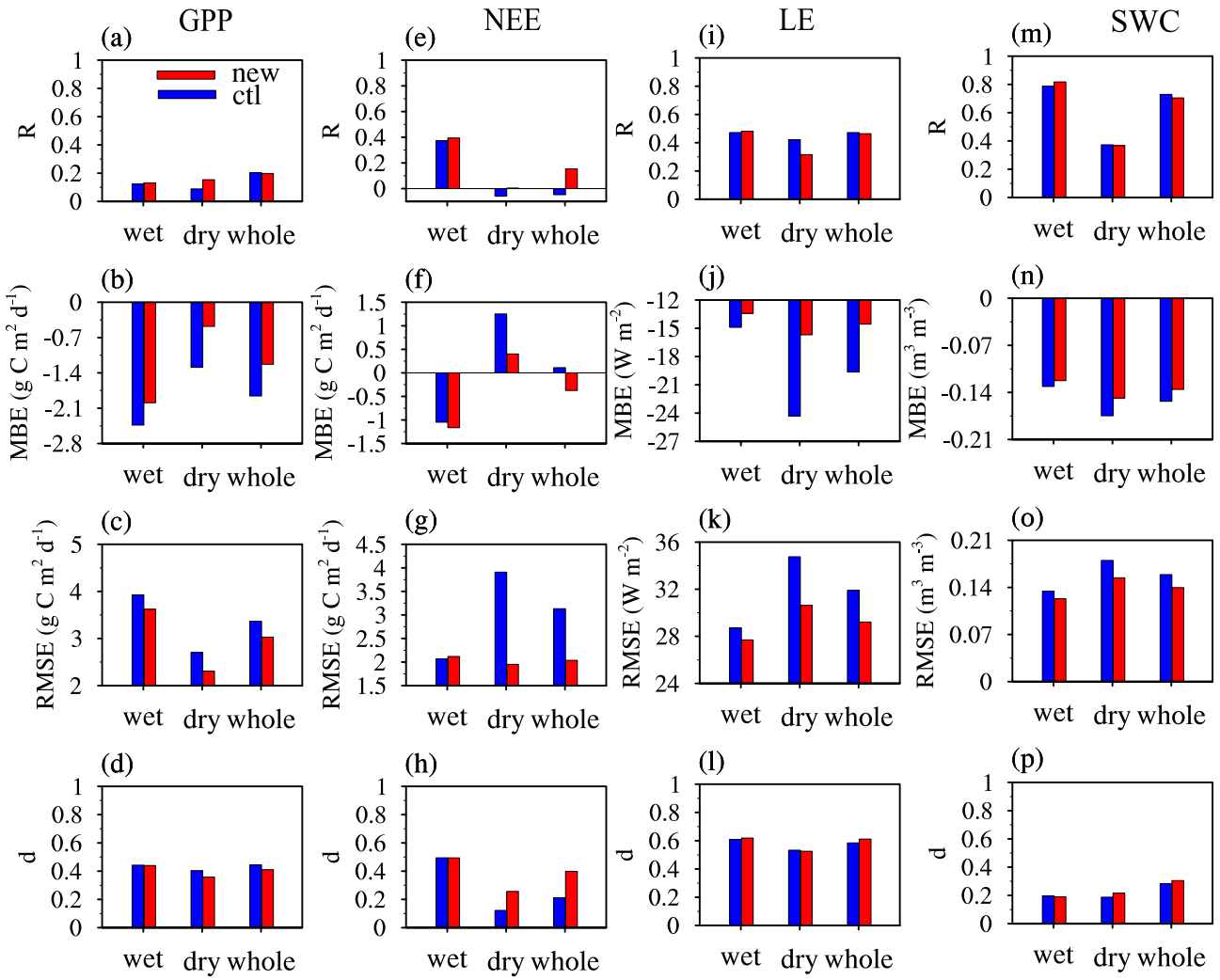

Fig. 7. Comparison between the results of CTL and NEW at the BRSa3 site for (a–d) GPP, (e–h) NEE, (i–l) LE, and (m–p) SWC (mean of 0–20 cm) compared with corresponding observations for wet months, dry months and the whole year. The four indices used are defined as Eq. (6–9) in section 2.4.

respectively. Figure 8 shows the annual cycle of simulated and observed GPP and LE averaged over the two study areas across 1982–2010, together with β_t. For R1, the dry season lasted four months: June–September. Both GPP and LE simulated by CTL showed obvious reductions due to the decreasing β_t (Fig. 8a) during the dry season, with large negative biases compared to observation (Figs. 8b and c). In contrast, the monthly variations of GPP and LE for NEW became smaller than those of CTL, with the RMSE reduced from 39.52 to 29.87 g C m^{-2} month^{-1} for GPP, and from 18.80 to 17.65 W m^{-2} for LE. During the dry season, the mean GPP and LE increased from 195.95 to 211.62 g C m^{-2} month^{-1}, and from 91.47 to 98.83 W m^{-2}, respectively–closer to the corresponding MTE observations. In R2, both simulated and observed GPP and LE were lower than that of R1 due to the difference of parameters for photosynthesis and transpiration between the two vegetation types (Figs. 8b and e). In this region the dry season was May–September, with β_t obviously decreasing from 1 to 0.6. During this period, both the two simulations showed significant decreases in GPP and LE, similar to observation, but too steep in CTL. In contrast, NEW showed similar improvements in GPP and LE in R2 as R1 (Figs. 8e and f), with the mean GPP increasing from 128.84 to 146.93 g C m^{-2} month^{-1}, and LE from 78.0 to 87.69 W m^{-2}, during June to September. Furthermore, the RMSE reduced from 65.70 to 54.42 g C m^{-2} month^{-1} for GPP, and from 22.0 to 19.62 W m^{-2} for LE, compared to observations. To summarize, the plant response to seasonal drought was better captured with a dynamic root distribution considered, though some divergence still remained.

In 2005, the Amazon experienced a severe drought— the worst for over a century (Saleska et al., 2007; Chen et al., 2009). Amazon rainfall reductions were the most extensive for July–September 2005 when the subtropical North Atlantic SST was at its highest (Zeng et al., 2008). Based on the 29-year climatology for 1982–2010 from CRUNCEP, the drought in 2005 was captured (Fig. 9a) and the black-boxed region with the largest negative precipitation anomaly

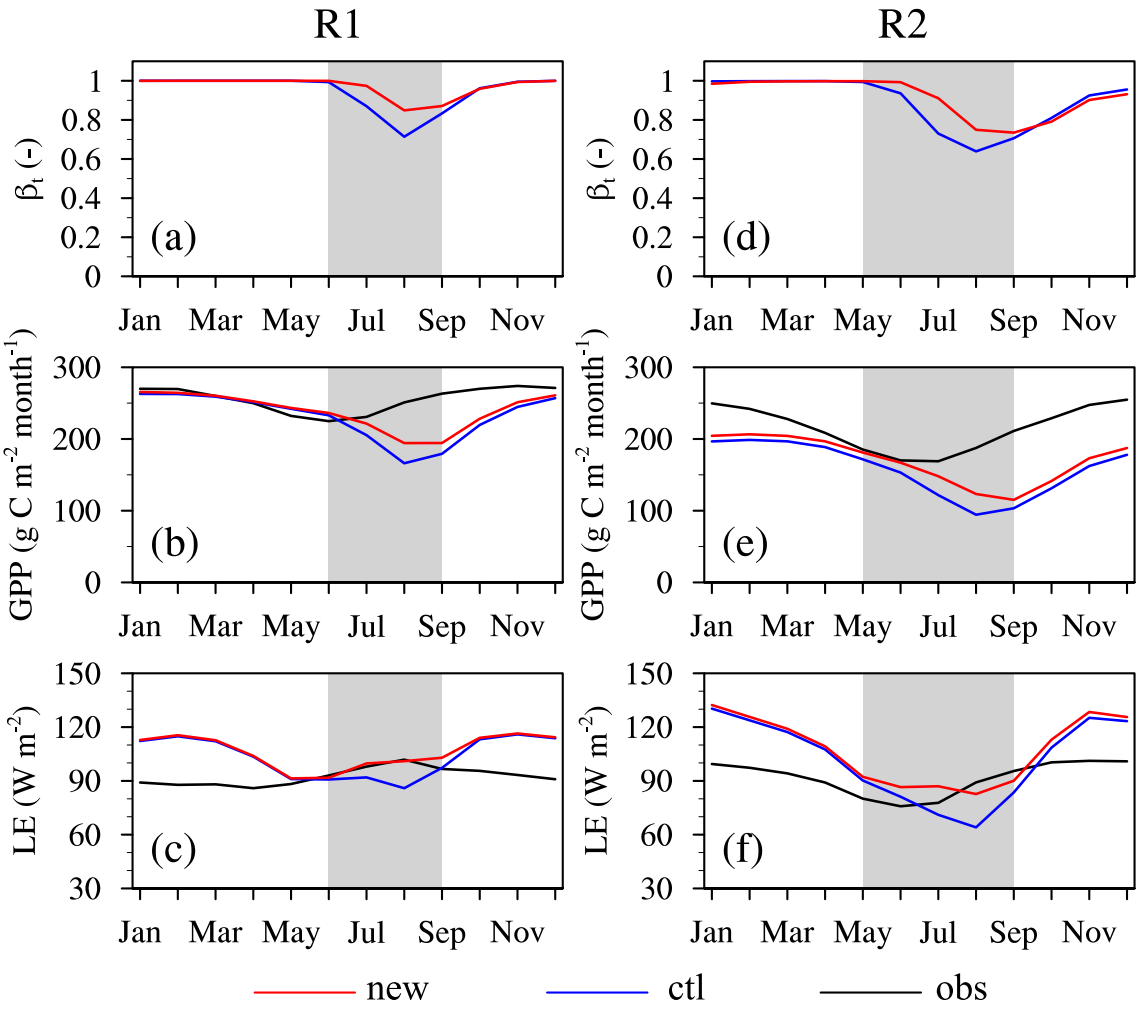

Fig. 8. Annual cycle of simulated β_t, GPP and LE, compared with their corresponding observations (MTE GPP and LE), averaged over the two study areas in the Amazon across 1982–2010: (a–c) for R1 and (d–f) for R2 (shaded areas indicate the dry season).

($\leqslant -50$ mm month^{-1}) was analyzed (hereafter R3). Figure 9b shows that the mean rainfall of R3 from July to September in 2005 was the lowest during the 29 years, at just 41.4 mm month^{-1}. Note that the 2005 rainfall anomaly based on CRUNCEP for 1982–2010 was similar to that for 1901–2010, but for temporal consistency only the former is shown and analyzed. Figures 9c–e show the annual cycle of simulated and observed GPP and LE averaged over R3 for 2005 and averaged across 1982–2010, together with β_t. During the 2005 drought, the simulated GPP and LE decreased in R3 (Figs. 9d and e), substantially lower than the observed multi-year average, but more rapidly in CTL than in NEW, especially in July–September, as a result of the decreasing β_t, indicative of more severe soil water stress (Fig. 9c). However, NEW mitigated the underestimation of GPP and LE in July–September during the 2005 drought by increasing the soil water availability, with the RMSE reduced from 30.3 to 23.1 g C m^{-2} month^{-1} for GPP and from 16.9 to 14.3 W m^{-2} for LE. In general, the vegetation response to the severe 2005 drought was better captured with a dynamic rooting scheme incorporated.

4. Conclusions and discussion

In this study, a dynamic rooting scheme that describes root growth as a compromise between water and N availability in the subsurface, was incorporated in CLM4.5-CN and its effects on C (GPP and NEE) and water cycle (LE and SWC) modeling were evaluated over the Amazon. At the BRSa3 site, the two simulations differed little in their results during the wet season. However, during the dry season (July–December), CTL underestimated GPP, LE and SWC, possibly as a result of the model's excessive sensitivity to drought. However, with the new rooting strategy, more root C was allocated into deeper soil layers and more water was able to be absorbed by the roots. This further reduced the soil water stress, and thus improved the C and water cycle modeling by reducing the RMSE in GPP by 0.4 g C m^{-2} d^{-1}, NEE by 1.96 g C m^{-2} d^{-1}, LE by 5.0 W m^{-2}, and SWC by 0.03 m^3 m^{-3}, compared with observations. Additionally, NEW was able to overcome part of the underestimation, indicating that a dynamic root distribution is not the only mechanism that needs to be considered. For the Amazon region, the default

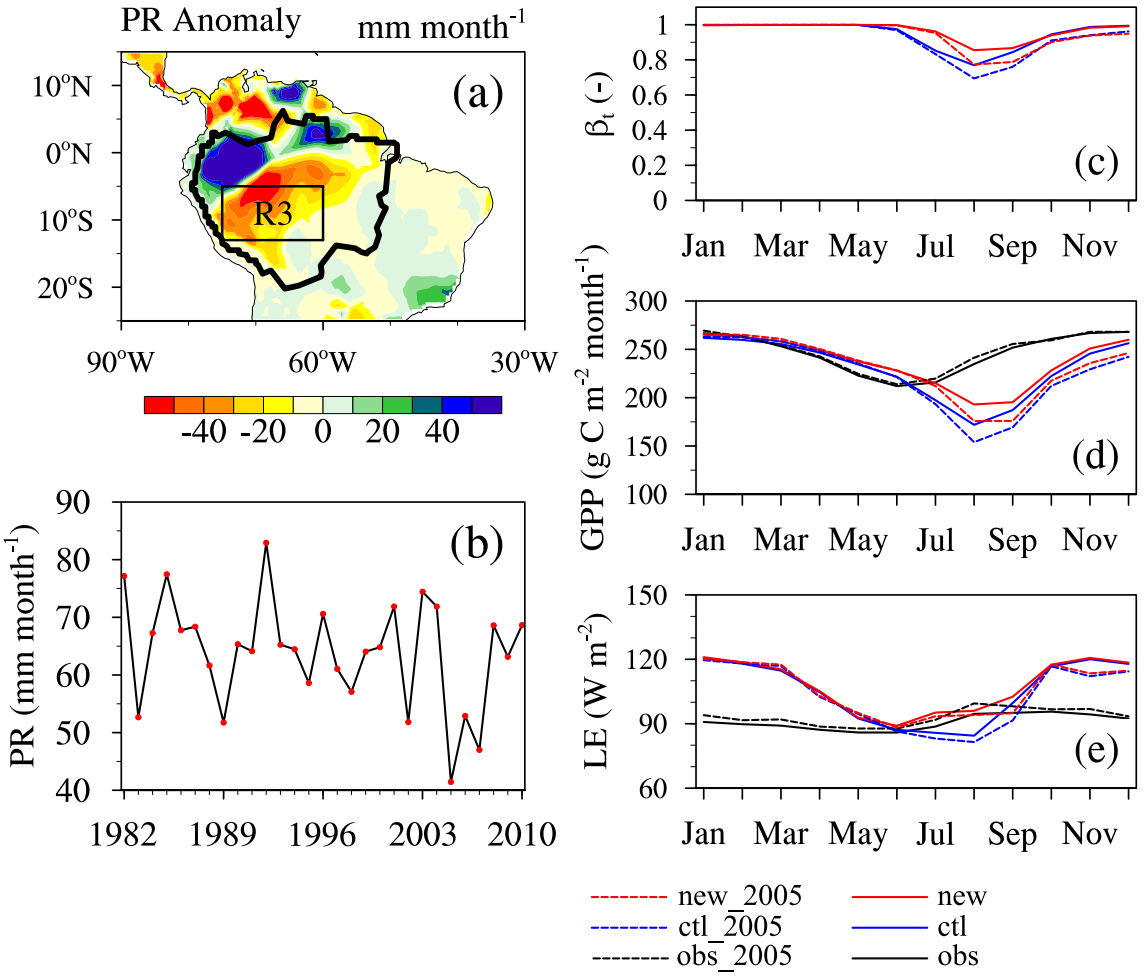

Fig. 9. (a) Monthly precipitation (PR) anomaly (units: mm month^{-1}) for July–September 2005, based on the 29-year climatology from 1982–2010 calculated from CRUNCEP (the black box represents the study region analyzed in section 3.3, denoted as R3). (b) Time series of monthly mean PR (units: mm month^{-1}) for July–September averaged over R3 from 1982–2010. (c–e) Annual cycle of simulated β_t, GPP and LE averaged over R3 for 2005 and averaged across 1982–2010, compared with their corresponding observations (MTE GPP and LE). The border of the Amazon is shown as a black line.

model showed obvious reductions in simulated GPP and LE due to the decreasing β_t during the dry season in both R1 and R2, with large negative biases. The C and water simulations were improved in NEW, with the RMSE for GPP reduced from 39.52 to 29.87 g C m^{-2} month^{-1} in R1, and from 65.70 to 54.42 g C m^{-2} month^{-1} in R2; and for LE, from 18.80 to 17.65 W m^{-2} in R1, and from 22.0 to 19.62 W m^{-2} in R2. In the severe 2005 drought, the region with the largest negative precipitation anomaly (R3) showed obvious decreases in GPP and LE – substantially lower than the observed multi-year average. The soil water availability during this period was able to be increased in NEW, and thus mitigated the underestimation of GPP and LE, with the RMSE reduced from 30.3 to 23.1 g C m^{-2} month^{-1} for GPP, and from 16.9 to 14.3 W m^{-2} for LE. In general, the vegetation response (including GPP and LE) to seasonal drought and the severe 2005 drought was better captured when a dynamic root distribution was incorporated, although some divergence still remained.

However, only including a dynamic root distribution is insufficient to improve the simulations to match observations, especially for SWC. To test the sensitivity of SWC to soil texture, we replaced the soil type using observational data from Li et al. (2012) and Yan and Dickinson (2014) at the BRSa3 site, where the soil type is mainly clay latosol (80% clay, 18% sand and 2% silt), into CLM4.5 instead of the IGBP data (35% clay, 45% sand and 20% silt). Thus, the water content at saturation (i.e. porosity) varied from 0.30 to 0.36 m^3 m^{-3}, and the saturated hydraulic conductivity varied from 0.021 to 0.019 mm s^{-1}. The simulation from observational soil types agreed better with ground-based SWC observations than that from the original IGBP data. The mean SWC of the top 0–20 cm increased from 0.34 to 0.42 m^3 m^{-3} for April, and from 0.20 to 0.30 m^3 m^{-3} for October (Figs. 10a and b). This suggests that soil texture is a critical factor for hydraulic properties, and observational soil type can reduce the biases of SWC simulations in CLM4.5.

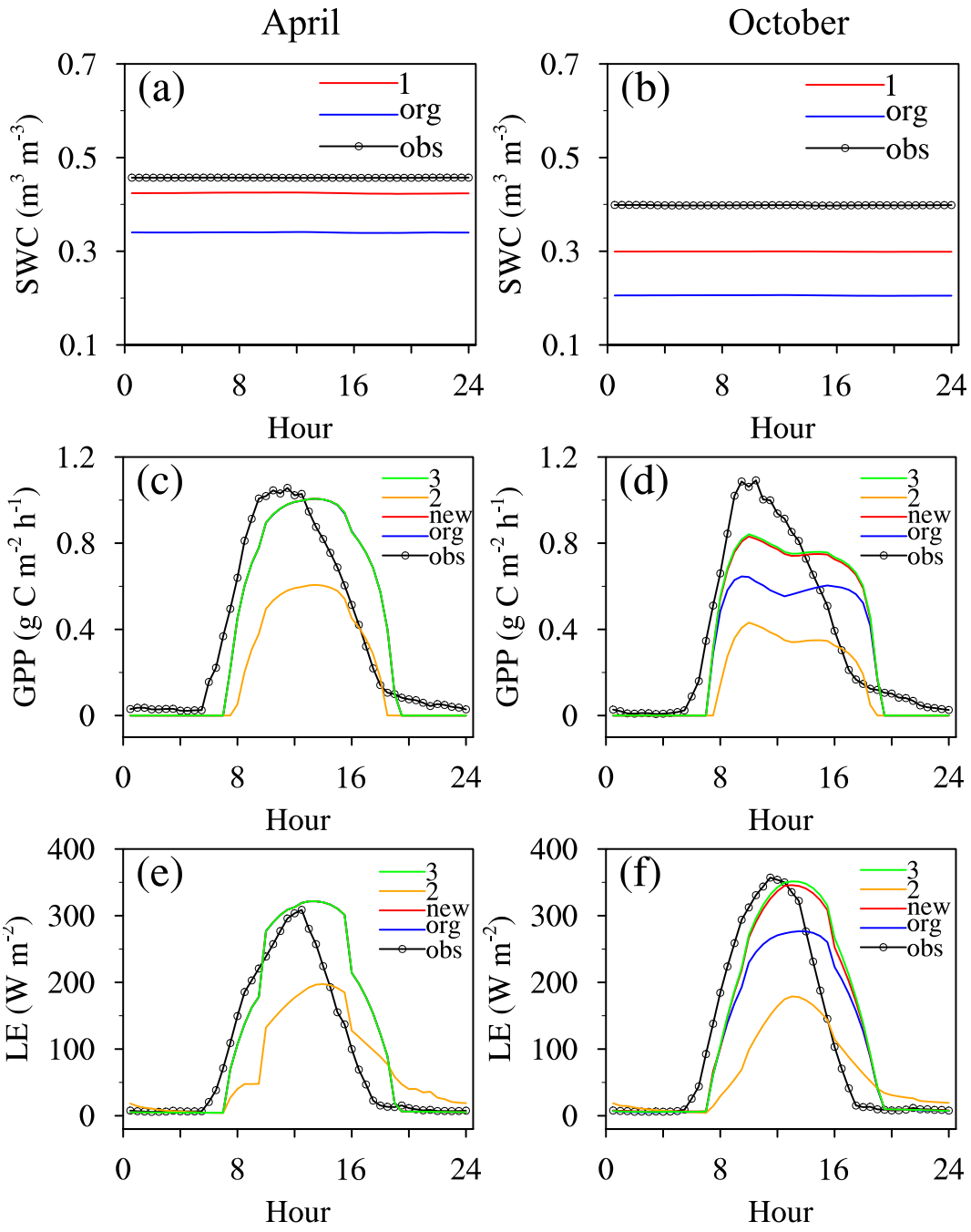

Fig. 10. (a, b) Sensitivity of SWC to different soil textures, and sensitivity of (c, d) GPP and (e, f) LE to different stomatal parameters and root profiles (obs, observation; org, the run with the original model; new, the run with the dynamic rooting scheme; 1, the run with observed soil texture; 2, the run with new stomatal parameters; 3, the run with the observed root profile).

The soil potential values (mm) when stomata are fully closed (ψ_c) or fully open (ψ_o) in CLM4.5, which are PFT-dependent, are from White et al. (2000). However, Verhoef and Egea (2014) found that the ψ_c and ψ_o values are not always realistic. In CLM4.5, ψ_c and ψ_o values of tropical broadleaf evergreen tree (the dominant PFT at the BRSa3 site) are −255 000 mm and −66 000 mm, respectively. To test the sensitivity of GPP and LE to different ψ_c and ψ_o values, we used another set of values (−127500 mm for ψ_c and −33000 mm for ψ_o) in the simulations. The results showed that the different ψ_c and ψ_o values caused large differences for the GPP and LE simulations (Figs. 10c–f).

To see if additional improvements could be made by using the observed root distribution data, another experiment (denoted as "3") was conducted for the BRSa3 site, in which the observed root distribution data were used to force CLM4.5. The results showed that the two runs (i.e. the new run and the run with observed root data) did not show large differ-

ences in GPP and LE during both the wet and dry seasons (Figs. 10c–f). This suggests that, in addition to the dynamic rooting scheme, many other root-related mechanisms, including deep root systems up to 18 m (Canadell et al., 1996), hydraulic redistribution (Ryel et al., 2002) and preferential root water uptake (Lai and Katul, 2000), also contribute to dry season water uptake and consequently drought responses, and should therefore be further examined in modeling studies. Previous studies (Tomasella et al., 2008; Miguez-Macho and Fan, 2012) suggest that groundwater in the Amazon can reduce wet season soil drainage and lead to larger soil water stores before the dry season arrives. This is one of the reasons for the observed absence of dry season water stress. In addition, more field observations and experiments will improve our understanding of how to represent root activities in plant physiological and ecological aspects (Yan and Dickinson, 2014). This paper presents only preliminary comparisons in the Amazon, and more analysis on the effects of a dynamic root distribution on eco-hydrological and climate modeling at the global scale is needed in the future.

Acknowledgements. This study was supported by the National Natural Science Foundation of China (Grant Nos. 41305066 and 41575096). The CRUNCEP and MTE data were downloaded freely from the NCAR (http://www.cesm.ucar.edu/) and Max Plank Institute for Biogeochemistry (https://www.bgc-jena.mpg.de/) websites, respectively. We also thank FLUXNET for providing valuable data for the BRSa3 site (http://ameriflux.lbl.gov/).

REFERENCES

Avissar, R., P. L. S. Dias, M. A. F. S. Dias, and C. Nobre, 2002: The large-scale biosphere-atmosphere experiment in Amazonia (LBA): Insights and future research needs. *J. Geophys. Res.*, **107**(D20), LBA 54-1–LBA 54-6, doi: 10.1029/2002JD002704.

Baker, I. T., L. Prihodko, A. S. Denning, M. Goulden, S. Miller, and H. R. da Rocha, 2008: Seasonal drought stress in the Amazon: Reconciling models and observations. *J. Geophys. Res.*, **113**(G1), G00B01, doi: 10.1029/2007JG000644.

Barlage, M., and X. B. Zeng, 2004: Impact of observed vegetation root distribution on seasonal global simulations of land surface processes. *J. Geophys. Res.*, **109**, D09101, doi: 10.1029/2003JD003847.

Bonan, G. B., 1996: Land surface model (LSM version 1.0) for ecological, hydrological, and atmospheric studies: Technical description and user's guide. Tech. Note NCAR/TN-417-STR, National Center for Atmospheric Research, Boulder, Colo.

Canadell, J., R. B. Jackson, J. B. Ehleringer, H. A. Mooney, O. E. Sala, and E. D. Schulze, 1996: Maximum rooting depth of vegetation types at the global scale. *Oecologia*, **108**(4), 583–595, doi: 10.1007/BF00329030.

Castillo, C. K. G., S. Levis, and P. Thornton, 2012: Evaluation of the new CNDV option of the Community Land Model: Effects of dynamic vegetation and interactive nitrogen on CLM4 means and variability. *J. Climate*, **25**, 3702–3714.

Chen, J. L., C. R. Wilson, B. D. Tapley, Z. L. Yang, and G. Y. Niu, 2009: 2005 drought event in the Amazon River basin as measured by GRACE and estimated by climate models. *J. Geophys. Res.*, **114**, B05404, doi: 10.1029/2008JB006056.

Coelho, F. E., and D. Or, 1999: A model for soil water and matric potential distribution under drip irrigation with water extraction by roots. *Pesquisa Agropecuária Brasileira*, **34**, 225–234.

Collins, D. B. G., and R. L. Bras, 2007: Plant rooting strategies in water-limited ecosystems. *Water Resour. Res.*, **43**, W06407, doi: 10.1029/2006WR005541.

Dickinson, R. E., M. Shaikh, R. Bryant, and L. Graumlich, 1998: Interactive canopies for a climate model. *J. Climate*, **11**, 2823–2836.

Drewry, D. T., P. Kumar, S. Long, C. Bernacchi, X. Z. Liang, and M. Sivapalan, 2010: Ecohydrological responses of dense canopies to environmental variability: 1. Interplay between vertical structure and photosynthetic pathway. *J. Geophys. Res.*, **115**(G4), 1–25.

El Maayar, M., and O. Sonnentag, 2009: Crop model validation and sensitivity to climate change scenarios. *Climate Research*, **39**(1), 47–59.

El Masri, B., S. J. Shu, and A. K. Jain, 2015: Implementation of a dynamic rooting depth and phenology into a land surface model: Evaluation of carbon, water, and energy fluxes in the high latitude ecosystems. *Agricultural and Forest Meteorology*, **211**–**212**, 85–99.

Fan, F. C., L. F. Zhang, Z. H. Li, S. Y. Liu, Y. F. Shi, and J. M. Jia, 2012: Response of root distribution of tomato to different irrigation methods in Greenhouse. *Journal of Hebei Agricultural Sciences*, **16**(8), 36–40, 44. (in Chinese)

Feddes, R. A., and Coauthors, 2001: Modeling root water uptake in hydrological and climate models. *Bull. Amer. Meteor. Soc.*, **82**, 2797–2810.

Hatzis, J. J., 2010: The development of a dynamic root distribution for the Community Land Model with carbon-nitrogen interactions. M.S. thesis, Northern Illinois University, Di Kalb, 184 pp.

Hodge, A., 2004: The plastic plant: Root responses to heterogeneous supplies of nutrients. *New Phytologist*, **162**, 9–24.

Hudiburg, T. W., B. E. Law, and P. E. Thornton, 2013: Evaluation and improvement of the Community Land Model (CLM4) in Oregon forests. *Biogeosciences*, **10**, 453–470.

Hutchings, M. J., and H. de Kroon, 1994: Foraging in plants: The role of morphological plasticity in resource acquisition. *Advances in Ecological Research*, **25**, 159–238.

Ichii, K., H. H. Hashimoto, M. A. White, C. Potter, L. R. Hutyra, A. R. Huete, R. B. Myneni, and R. R. Nemani, 2007: Constraining rooting depths in tropical rainforests using satellite data and ecosystem modeling for accurate simulation of gross primary production seasonality. *Global Change Biology*, **13**, 67–77, doi: 10.1111/j.1365-2486.2006.01277.x.

Ivanov, V. Y., R. L. Bras, and E. R. Vivoni, 2008: Vegetation-hydrology dynamics in complex terrain of semiarid areas: 1. A mechanistic approach to modeling dynamic feedbacks. *Water Resour. Res.*, **44**, W03429, doi: 10.1029/2006WR005588.

Jackson, R. B., H. A. Mooney, and E. D. Schulze, 1997: A global budget for fine root biomass, surface area, and nutrient contents. *Proceedings of the National Academy of Sciences of the United States of America*, **94**, 7362–7366.

Jackson, R. B., J. Canadell, J. R. Ehleringer, H. A. Mooney, O. E. Sala, and E. D. Schulze, 1996: A global analysis of root distributions for terrestrial biomes. *Oecologia*, **108**, 389–411.

Jing, C. Q., L. Li, X. Chen, and G. P. Luo, 2014: Comparison of

root water uptake functions to simulate surface energy fluxes within a deep-rooted desert shrub ecosystem. *Hydrological Processes*, **28**, 5436–5449.

Jung, M., M. Reichstein, and A. Bondeau, 2009: Towards global empirical upscaling of FLUXNET eddy covariance observations: Validation of a model tree ensemble approach using a biosphere model. *Biogeosciences*, **6**, 2001–2013.

Jung, M., and Coauthors, 2011: Global patterns of land-atmosphere fluxes of carbon dioxide, latent heat, and sensible heat derived from eddy covariance, satellite, and meteorological observations. *J. Geophys. Res.*, **116**, G00J07, doi: 10.1029/2010JG001566.

Lai, C. T., and G. Katul, 2000: The dynamic role of root-water uptake in coupling potential to actual transpiration. *Advances in Water Resources*, **23**, 427–439.

Lawrence, D. M., and Coauthors, 2011: Parameterization Improvements and Functional and Structural Advances in Version 4 of the Community Land Model. *Journal of Advances in Modeling Earth Systems*, **3**, M03001.

Lawrence, P. J., and T. N. Chase, 2007: Representing a new MODIS consistent land surface in the Community Land Model (CLM 3.0). *J. Geophys. Res.*, **112**, G01023, doi: 10.1029/2006JG000168.

Le, P. V. V., P. Kumar, D. T. Drewry, and J. C. Quijano, 2012: A graphical user interface for numerical modeling of acclimation responses of vegetation to climate change. *Computers & Geosciences*, **49**, 91–101, doi: 10.1016/j.cageo.2012.07.007.

Li, F., S. Levis, and D. S. Ward, 2013: Quantifying the role of fire in the Earth system-Part 1: Improved global fire modeling in the Community Earth System Model (CESM1). *Biogeosciences*, **10**, 2293–2314, doi: 10.5194/bg-10-2293-2013.

Li, L. H., Y. P. Wang, Q. Yu, B. Pak, D. Eamus, J. Yan, E. van Gorsel, and I. T. Baker, 2012: Improving the responses of the Australian community land surface model (CABLE) to seasonal drought. *J. Geophys. Res.*, **117**, G04002, doi: 10.1029/2012JG002038.

Li, X. M., C. X. Xu, and S. M. Su, 1998: Affection of deep ditch manuring method to apple root system pattern in arid farming orchard. *Acta Botanica Boreali-Occidentalia Sinica*, **18**(4), 590–594. (in Chinese)

Marthews, T. R., C. A. Quesada, D. R. Galbraith, Y. Malhi, C. E. Mullins, M. G. Hodnett, and I. Dharssi, 2014: High-resolution hydraulic parameter maps for surface soils in tropical South America. *Geoscientific Model Development*, **7**, 711–723.

McMurtrie, R. E., C. M. Iversen, R. C. Dewar, B. E. Medlyn, T. Näsholm, D. A. Pepper, and R. J. Norby, 2012: Plant root distributions and nitrogen uptake predicted by a hypothesis of optimal root foraging. *Ecology and Evolution*, **2**(6), 1235–1250.

Miguez-Macho, G., and Y. Fan, 2012: The role of groundwater in the Amazon water cycle: 2. Influence on seasonal soil moisture and evapotranspiration. *J. Geophys. Res.*, **117**, D15114, doi: 10.1029/2012JD017540.

Nepstad, D. C., and Coauthors, 1994: The role of deep roots in the hydrological and carbon cycles of Amazonian forests and pastures. *Nature*, **372**, 666–669.

Oleson, K. W., and Coauthors, 2010: Technical description of version 4.0 of the Community Land Model (CLM). NCAR Tech. Note NCAR/TN-478+STR, National Center for Atmospheric Research, 257 pp.

Oleson, K. W., and Coauthors, 2013: Technical description of version 4.5 of the Community Land Model (CLM). NCAR Tech. Note NCAR/TN-503+STR, National Center for Atmospheric Research, 420 pp.

Ryel, R., M. Caldwell, C. Yoder, D. Or, and A. Leffler, 2002: Hydraulic redistribution in a stand of *Artemisia tridentata*: Evaluation of benefits to transpiration assessed with a simulation model. *Oecologia*, **130**(2), 173–184, doi: 10.1007/s004420100794.

Saleska, S. R., K. Didan, A. R. Huete, and H. R. da Rocha, 2007: Amazon forests green-up during 2005 drought. *Science*, **318**, 612.

Schenk, H. J., 2008: The shallowest possible water extraction profile: A null model for global root distributions. *Vadose Zone Journal*, **7**, 1119–1124.

Schenk, H. J. and R. B. Jackson, 2002: The global biogeography of roots. *Ecological Monographs*, **72**(3), 311–328.

Shangguan, W., Y. J. Dai, Q. Y. Duan, B. Y. Liu, and H. Yuan, 2014: A global soil data set for earth system modeling. *Journal of Advances in Modeling Earth Systems*, **6**, 249–263.

Sivandran, G., and R. L. Bras, 2013: Dynamic root distributions in ecohydrological modeling: A case study at Walnut Gulch Experimental Watershed. *Water Resour. Res.*, **49**, 3292–3305, doi: 10.1002/wrcr.20245.

Smithwick, E. A. H., M. S. Lucash, M. L. McCormack, and G. Sivandran, 2014: Improving the representation of roots in terrestrial models. *Ecological Modelling*, **291**, 193–204.

Tomasella, J., M. G. Hodnett, L. A. Cuartas, A. D. Nobre, M. J. Waterloo, and S. M. Oliveira, 2008: The water balance of an Amazonian micro-catchment: The effect of interannual variability of rainfall on hydrological behaviour. *Hydrological Processes*, **22**, 2133–2147, doi: 10.1002/hyp.6813.

Verhoef, A., and G. Egea, 2014: Modeling plant transpiration under limited soil water: Comparison of different plant and soil hydraulic parameterizations and preliminary implications for their use in land surface models. *Agricultural and Forest Meteorology*, **191**, 22–32.

Viovy, N., 2011: CRUNCEP data set [Description available at http://dods.extra.cea.fr/data/p529viov/cruncep/readme.htm. Data available at http://dods.extra.cea.fr/store/p529viov/cruncep/V4_1901_2012/].

Warren, J. M., P. J. Hanson, C. M. Iversen, J. Kumar, A. P. Walker, and S. D. Wullschleger, 2015: Root structural and functional dynamics in terrestrial biosphere models-evaluation and recommendations. *New Phytologist*, **205**, 59–78.

Weaver, J. E., 1926: *Root Development of Field Crops*. McGraw-Hill Book Co., New York & London, 291 pp.

White, M. A., P. E. Thornton, S. W. Running, and R. R. Nemani, 2000: Parameterization and sensitivity analysis of the BIOME-BGC terrestrial ecosystem model: Net primary production controls. *Earth Interactions*, **4**, 1–85.

Yan, B. Y., and R. E. Dickinson, 2014: Modeling hydraulic redistribution and ecosystem response to droughts over the Amazon basin using Community Land Model 4.0 (CLM4). *J. Geophys. Res.*, **119**, 2130–2143, doi: 10.1002/2014JG002694.

Yuan, X., and X. Z. Liang, 2011: Evaluation of a Conjunctive Surface-Subsurface Process model (CSSP) over the contiguous United States at regional-local scales. *Journal of Hydrometeorology*, **12**, 579–599, doi: 10.1175/2010JHM1302.1.

Zeng, N., J. H. Yoon, J. A. Marengo, A. Subramaniam, C. A. Nobre, A. Mariotti, and J. D. Neelin, 2008: Causes and impacts of the 2005 Amazon drought. *Environmental Research Letters*, **3**, 014002, doi: 10.1088/1748-9326/3/1/014002.

Zeng, X. B., 2001: Global vegetation root distribution for land modeling. *Journal of Hydrometeorology*, **2**(5), 525–530.

Zeng, X. B., M. Shaikh, Y. J. Dai, R. E. Dickinson, and R. Myneni, 2002: Coupling of the common land model to the NCAR community climate model. *J. Climate*, **15**, 1832–1854.

Zeng, X. B., Y. J. Dai, R. E. Dickinson, and M. Shaikh, 1998: The role of root distribution for climate simulation over land. *Geophys. Res. Lett*., **25**, 4533–4536.

Zheng, Z., and G. L. Wang, 2007: Modeling the dynamic root water uptake and its hydrological impact at the Reserva Jaru site in Amazonia. *J. Geophys. Res*., **112**, G04012, doi: 10.1029/2007JG000413.